Recovering Stereo Pairs from Anaglyphs

Armand Joulin
INRIA/Ecole Normale Supérieure[1]
armand.joulin@inria.fr

Sing Bing Kang
Microsoft Research
sbkang@microsoft.com

Abstract

An anaglyph is a single image created by selecting complementary colors from a stereo color pair; the user can perceive depth by viewing it through color-filtered glasses. We propose a technique to reconstruct the original color stereo pair given such an anaglyph. We modified SIFT-Flow and use it to initially match the different color channels across the two views. Our technique then iteratively refines the matches, selects the good matches (which defines the "anchor" colors), and propagates the anchor colors. We use a diffusion-based technique for the color propagation, and added a step to suppress unwanted colors. Results on a variety of inputs demonstrate the robustness of our technique. We also extended our method to anaglyph videos by using optic flow between time frames.

1. Introduction

Arguably, the first 3D motion picture was shown in 1889 by William Friese-Green, who used the separation of colors from the stereo pair to generate color composites. Glasses with appropriate color filters are used to perceive the depth effect. Such images generated by color separation are called anaglyphs. An example is shown in top-left part of Figure 1, where the color separation is red-cyan. Here, anaglyph glasses comprising red-cyan filters are used to perceive depth. There is much legacy anaglyph content available with no original color pairs.

In this paper, we show how we can reliably reconstruct a good approximation of the original color stereo pair given its anaglyph. We assume the left-right color separation is red-cyan, which is the most common; the principles of our technique can be applied to other color separation schemes.

Given an anaglyph, recovering the stereo color pair is equivalent to transferring the intensities in the red channel to the right image and the intensities in the blue and green channels to the left one. Unfortunately, the intensity distributions between the three channels are usually very different, with mappings of intensities typically being many-to-many. This complicates the use of stereo and standard color transfer methods. Since the input is essentially a stereo pair, we have to handle occlusions as well.

Our technical contributions are as follow:

- A completely automatic technique for reconstructing the stereo pair from an anaglyph (image or video).
- Non-trivial extensions to SIFT-Flow [14] to handle registration across color channels.
- Non-trivial extensions to Levin et al.'s [11] colorization technique to handle diffusion of only specific color channels per view, and use of longer range influence. We also added the step of suppressing visually inappropriate colors at disocclusions.

We made the following assumptions:

- There are no new colors in the disoccluded regions.
- The information embedded in the anaglyph is enough to reconstruct full rgb[2].
- The images are roughly rectified (with epipolar deviation of up to ± 25 pixels).

As we demonstrate through a variety of results, our technique is robust to inadvertent asymmetric occlusion in one camera (e.g., part of a finger in one view but not in the other) as well as blurry and low-light scenes.

2. Related work

As far as we know, there are two approaches for generating stereo pairs from anaglyphs. The first is a tool called *Deanaglyph*[3]. However, it requires as input not just the anaglyph, but also one color image. Dietz [3] proposed a method to recover the original images from anaglyphs captured using a modified camera with color filters. There is unfortunately insufficient information in the paper on how his technique works; however, his results show that the colors often do not match across the reconstructed stereo pair.

[1]WILLOW project-team, Laboratoire d'Informatique de l'Ecole Normale Supérieure, ENS/INRIA UMR 8548.

[2]Certain types of anaglyphs, such as the "optimized" anaglyph, throws away the red channel; it fakes the red channel of the left image by combining green and blue channels.

[3]http://www.3dtv.at/Knowhow/DeAnaglyph_en.aspx

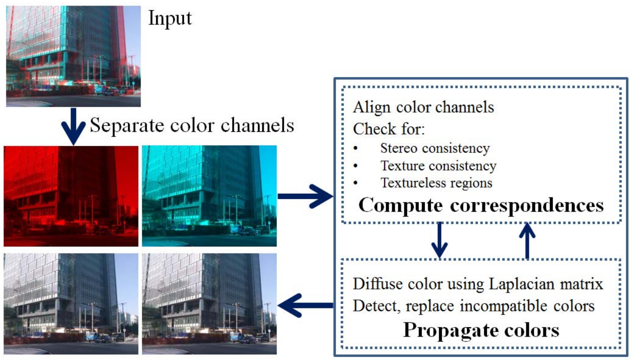

Figure 1. Our pipeline: Given an anaglyph, we iteratively find correspondences between the left and right images and recolorize the two images based on these correspondences.

Another paper which is closely related is that of Bando et al. [1]. They use an RGB color filter on the camera lens aperture to obtain three known shifted views. They propose an algorithm to match the corresponding pixels across the three channels by exploiting the tendency of colors in natural images to form elongated clusters in the RGB space (color lines model of [16]), with the assumption of small disparities (between -5 to 10 pixels only).

We now briefly survey topics relevant to our approach: colorization, extraction of dense correspondences, and color transfer.

2.1. Colorization

In our approach, we use a diffusion-based colorization method to propagate the colors of reliable correspondences to other pixels. Colorization methods assume that the color of some input pixels is known and infer the color of the other pixels [11, 15, 22, 12, 20, 9]. Most colorization methods also assume, explicitly or implicitly, that the greyscale values are known and used as part of the optimization. For anaglyphs, the luminance values are not available.

Our method is based on diffusion of reliably transferred colors using a graph construct (e.g., diffusing reliable red intensities in the left view). Our approach is related to [11]. They assume that the input colors given by a user are approximate and may be refined depending on the image content. In our work, this assumption is not required. Unlike [11], since we work in rgb space directly, we must preserve edges while diffusing the color (especially over shadowed regions). We use *longer-range information* (for each pixel, within a 21×21 centered window) to diffuse colors.

Another popular approach to colorize an image is to use the geodesic of an image to connect a pixel with unknown color to an input pixel [22]. This type of approach works well in practice but implicitly assumes the number of input pixels is small, which is not true in our case.

2.2. Dense correspondences

Our approach relies on finding dense good correspondences between both images. Our approach adapted the techniques of SIFT-flow [14] and optical flow [13] to fit the requirements of our problem.

There are many methods designed to compute dense correspondences between images. Most stereo matching methods have been proven to be successful when the cameras are radiometrically similar [19]. These are not applicable in our case, since we are matching the red channel in one view with cyan in the other. There are also approaches that handle changes in exposure [10, 7] or illumination [6]. However, such approaches typically assume a bijective mapping between the two intensity maps, which is violated for anaglyphs.

Bando et al. [1] use *Markov random field* to register across color channels. As mentioned earlier, it is important to note that their assumption of local cluster shape similarity based on the color lines model [16] is facilitated by small disparities.

More recently, HaCohen et al. [5] have proposed a color transfer method based on local correspondence between similar images. They look for correspondences between images with different light conditions and taken by different cameras. Unlike graph matching based approaches, their approach finds correspondences with no spatial constraints. In our work, the two images to be reconstructed are highly spatially related; ignoring this information leads to incorrect colorization.

2.3. Color transfer

A related subject of interest is color transfer, which is the process of modifying the color of a target image to match the color characteristics of a source image. Most approaches [18, 21, 4, 17] assume that at least the target image is in color (or at least greyscale). As a result, they are not directly applicable in our case. These approaches tend to make use of global statistics of the image and thus may be less effective in recovering the true color locally.

3. Overview of our approach

Our approach to recover the stereo pair from an anaglyph is to iteratively find dense good correspondences between the two images and recolorizing them based on these correspondences. As a post-processing stage, we detect "incompatible" colors in unmatched regions (defined as colors that exist in one image but not the other) and assign them to the nearest known colors. This process prevents new colors from appearing in the occluded regions.

Figure 1 summarizes our process. We use a modified version of SIFT-Flow to obtain an initial set of correspondences between the two images. We then recolorize the images

Ground truth SIFT-Flow ASIFT-Flow (ours)

Figure 2. Comparison between the original SIFT-Flow and our version. Notice the incorrect colors transferred for the original SIFT-Flow in the darker lower region.

Anaglyph [10] [5] Ours

Figure 3. Comparison between different algorithms in terms of reconstruction. We implemented the algorithm described in [10] and used the online code of [5].

based on these correspondences. Each channel is then iteratively matched *independently* using an optical flow method to produce new good correspondences; the colors are updated using the new correspondences.

In the next section, we describe the dense matching algorithms to align the color channels of the two images. We then explain how we retrieve good correspondences from this alignment.

4. Channel alignment

Given a red-cyan anaglyph, we first need to align the red channel with the blue and green channels. To accomplish this, we use two different graph matching algorithms, namely, modified versions of SIFT-Flow and an optical flow algorithm. We chose SIFT-Flow [14] because it is capable of locally matching images with different intensity distributions.

4.1. Initial rough channel alignment

SIFT-Flow is used to compute correspondences between the initially color-separated images. The intuition is that despite brightness variability across the color channels, there is usually a strong correlation in local texture. SIFT is used because it is some form of a texture descriptor and it is inherently invariant to some amount of brightness changes.

We denote by L and R the left and right images respectively. Given pixel $p = (x, y)$ of the left image (resp. right image), we denote by $S_L(p)$ (resp. $S_R(p)$) its associated SIFT feature. SIFT-Flow maps pixels of a source image to those in a target image while maintaining the local structure of the input image. More precisely, given the left image as the input, for each pixel p, SIFT-Flow tries to find the best disparity $d(p) = (d_x(p), d_y(p))$ as to match $S_L(p)$ to $S_R(p + d(p))$ by minimizing

$$\begin{aligned} E_{SF} \;=\; & \sum_{p \in L} \|S_L(p) - S_R(p + d(p))\|_1 + \\ & \frac{1}{\sigma^2} \sum_p \|d(p)\|_2 + \\ & \sum_{p \sim q} \min(\alpha|d_x(p) - d_x(q)|, t_x) + \\ & \quad \min(\alpha|d_y(p) - d_y(q)|, t_y), \end{aligned} \tag{1}$$

where σ, α are constants and t_x and t_y are thresholds on the maximum disparity beyond which there is a penalty. We set $t_x = 5$, $t_y = 2$, $\sigma = 14$ and $\alpha = 2$.

SIFT-Flow is originally used to match scenes based on context. In our case, the scenes to be matched are the same, just shown as shifted versions and in different color bands. Unfortunately, the original SIFT-Flow tends to not do well in less textured regions, which often results in artifacts if used as is for matching followed by color transfer. These two observations led us to adapt SIFT-Flow to our problem (which we will now refer to as "anaglyph SIFT-Flow" or ASIFT-Flow).

ASIFT-Flow. SIFT flow is designed to match very different images. Each given pixel p is associated with a search window $W(p)$. Typically, in the original SIFT-Flow, this window is square and cover most of the image. In our case, the images are very similar and roughly rectified, and as a result shifts are along the x-axis. We thus restrict the window $W(p)$ to a $\frac{w}{12} \times w$ rectangle along the x-axis, where w is the width of the image (typically $w = 640$, leading to a 50×640 search window).

SIFT-Flow directly matches SIFT features which are known to have a higher value on highly texture regions which encourage matching of highly texture regions over low texture ones. This introduces strong alignment errors in dark or blurry regions (see Figure 2). Notice the artifacts for SIFT-Flow at the darker lower region caused by incorrect color transfer.

We handle this problem by using a mapping ϕ related to a Hellinger kernel on the SIFT features. More specifically, given a SIFT feature $S(p) = (S_d(p))_{d \leq D_S}$ of dimension D_S, its Hellinger mapping is a D_S dimensional vector $F(p)$ with d-th coordinate equal to

$$F_d(p) = \sqrt{\frac{S_d(p)}{\sum_{d'=1}^{D_S} S_{d'}(p)}}. \tag{2}$$

We replace in Eq. 1 the SIFT features by their Hellinger mapping. This mapping assigns more weight to regions with smaller gradients, leading to our result in Figure 2.

Finally, in the original SIFT-flow method, the cost of matching a pixel to the outside of the target image is independent of its proximity to the left and right borders of the image. In other terms, SIFT-Flow penalize the matching of a pixel p to the outside by a constant cost K. In our case, since we expect our image pair to be roughly rectified, disparity is mostly horizontal. As such, we penalize vertical shifts as well as based on the amount of deviation from the left or right borders. More precisely, given a pixel p at a L_1 distance $d(p)$ to the closest border, we replace the constant cost K by a cost depending on this distance, namely, $Kd(p)$.

Comparison with other matching methods. Why did we use ASIFT-Flow and not other methods? In particular, Kim et al. [10] propose a stereo matching algorithm which works for images with different intensity distribution. However, they assume that the mapping of intensity levels is one-to-one, which is not true in general between color channels. HaCohen et al. [5] recover the various textures of the image but is not robust enough to deal with high intensity changes resulting in wrong color estimations. We find that these two approaches do not work as well as ASIFT-Flow; a representative example is shown in Figure 3.

SIFT is computed on 16×16 patches; its coarseness is why we use it only to obtain a first rough alignment in the initialization. In the next section, we explain how we refine the channel alignment.

4.2. Refining channel alignment

Using the matches by ASIFT-Flow, we have a first rough colorization of the two images. In many cases, the results look reasonable. However, artifacts can occur in areas with significant lighting and/or texture changes. In addition, since ASIFT-Flow is block-based, artifacts are usually generated at object boundaries.

Unfortunately, since the color reconstruction is still only approximate, image rectification may only be approximate as well. As a result, we allow for some slop in the vertical direction when refining the search, and we use optical flow. Note that our problem is not that of stereo, but rather color reconstruction. We compute optical flow *independently* on the three channels, namely, the red channel for the left image and the blue and green channels for the right image. While some of the re-estimated matches are better, errors still occur. In the next section, we describe a criteria to select the good matches.

5. Finding good matches

Given matches from left to right $M_{L\mapsto R}$ and those from right to left $M_{R\mapsto L}$, different criteria can be used to select the more reliable ones. We use three different criteria: stereo consistency, texture consistency, and detection of textureless regions. These criteria are based on comparing an original known channel with its reprojected (warped) version ($M_{L\mapsto R}$ and $M_{R\mapsto L}$).

Stereo consistency (or match reciprocity). This refers to the property that for a pair of correspondences, in each direction, the corresponding pixel is the best choice. In other words, given a pixel i in the left image, we say that it is a good match wrt stereo consistency if $i == M_{R\mapsto L}\big(M_{L\mapsto R}(i)\big)$.

Since the imprecision in SIFT matching at the pixel level makes it difficult to satisfy this criterion exactly, we use a soft version where a pixel is allow to match a pixel within a $t_x \times t_y$ $(= 5 \times 2)$ window. The modified criteria are

$$|x(i) - x(M_{R\mapsto L}\big(M_{L\mapsto R}(i)\big))| \leq t_x, \tag{3}$$

$$|y(i) - y(M_{R\mapsto L}\big(M_{L\mapsto R}(i)\big))| \leq t_y. \tag{4}$$

Texture consistency. A match is good if its reprojected (warped) value is similar to the observed. In this case, we are comparing SIFT features: original observed $S(p)$ and reprojected $\hat{S}(p)$. The match is deemed good the distance between the two features is small enough, i.e., $|S(p) - \hat{S}(p)| < t_s$. Typically, we fix $t_s = 2$.

Textureless regions. Textureless regions are a special case, since both our rough and refined alignment steps tend to fail there. We define a pixel to be "textureless" if its associated SIFT feature has a norm below a certain threshold (set to 1). A match is deemed good if both pixels are textureless.

The criteria allow us to select good candidate matches. We make the strong assumption that the reconstructed colors (*anchor* colors) using these matches is correct. Our goal is now to propagate anchor colors to the other pixels, which is the colorization step.

6. Colorization

There are many approaches for colorization [8, 22, 11, 2]. The most popular are either based on diffusion [11] or geodesic distance [22]. We did not consider methods based on geodesic distance because they are not suitable for cases where the number of anchor pixels (i.e., good matches in our case) is very high. Based on our experiments, they occupy between 80-90% of the image.

In this section, we describe a colorization method inspired by Levin et al. [11]; non-trivial modifications are necessary to adapt to our unique problem formulation.

6.1. Diffusion method

In Levin et al. [11], given a greyscale image, a similarity matrix W between nearby pixels is constructed, from which a diagonal matrix D containing the sum of each row of W and a normalized Laplacian matrix $L = I - D^{-1}W$ are computed and used for color diffusion. Denoting by $I(i)$ the intensity of a given pixel, we use W with entry W_{ij}

being zero if the two pixels i and j are not within 10 pixels of each other; otherwise it is

$$W_{ij} = \exp(-\gamma \|I(i) - I(j)\|_2^2)\delta(\|I(i) - I(j)\|_1 \leq \lambda_I),$$

where δ is the indicator (membership) function and λ_I is a fixed threshold set to 25. The anchor colors (y_k, "known") are fixed, with the rest (y_u, "unknown") needed to be computed. Let L_{uu} (resp. L_{uk}) be the sub-block matrix of L with row and column indexed by the unknown pixels (respectively unknown and known pixels). We solve

$$\min_{y_u \in [0,1]} \frac{1}{2}(y_u^T L_{uu} y_u + 2 y_u L_{uk} y_k),$$

which is equivalent to the following linear problem:

$$L_{uu} y_u = L_{uk} y_k.$$

If N_p is the number of unknown pixels, solving the linear problem is $O(N_p^2)$. For most images, N_p is small and this closed form solution is efficiently computed. For large images or video sequences, N_p can be very big and computing the closed form solution is prohibitive. In those cases, we reduce the complexity of the algorithm by considering N_r non-overlapping horizontal bands (we use $N_r = 4$). This is guaranteed to converge since the cost function is strongly convex and the complexity is $O(N_r N_p)$.

6.2. Differences with Levin et al. [11]

In [11], the user-specified colors may be modified. This is reasonable, since they are specified via scribbles, which are only approximate. Their method can be regarded as a one-step gradient descent with a good initialization. In addition, their method works in YUV space because the grayscale image is known. In our case, the grayscale image is unknown, and as such, this color space is not useable. Finally, our similarity matrix is different. More specifically, for [11], the similarity function is different and only immediate 4-neighbors are connected. This is justified in the YUV space but does not work as well in rgb space.

We iterate between colorizing both images and aligning the channels. At the end of this process, it is possible for disoccluded regions to have colors not found elsewhere (we term such colors as "incompatible" colors). In the next section, we describe a method to detect such colors and recolorize them.

7. Detecting incompatible colors

Our approach uses the anchor colors to fill in the missing colors. However, objects in disoccluded regions may be incorrectly colored. As shown in Figure 4, for each scene, a border region of the leftmost image is unobserved in the other view, resulting in out-of-place colorization. To detect such occurrences and subsequently color correct, we make the assumption that there are no new colors in the occluded regions in order to produce visually plausible outputs.

Figure 4. Examples of recolorization of occluded regions with incompatible colors.

To recolorize, we first detect regions with incompatible colors before we recolorize them with longer range connections. Let us first consider the right image; the same reasoning is applied to the left image. Given pixel p in the right image with color $c_p = (\hat{r}_p, g_p, b_p)$, the goal is to find if its estimated red value $\hat{r}_p$ is compatible with the red values observed in the rest of the image given the same blue and green values.

While it seems natural to compute $P(\hat{r}_p \mid g_p, b_p)$ on the good matches, the function will not be precise because the samples are small given the wide range of blue and green values. In addition, it is not clear how to define a threshold over the probability values. Instead, we consider the Nadaraya-Watson kernel regressor to estimate the most probable red value the pixel p should have given its current estimate. The estimator is

$$r_p^{NW} = \sum_{q \in \mathcal{Q}} \left(\frac{K(\frac{\hat{r}_p - r_q}{h})}{\sum_{q \in \mathcal{Q}} K(\frac{\hat{r}_p - r_q}{h})} \right) r_q, \tag{5}$$

where K is a kernel with bandwidth $h = 0.1$ and $\mathcal{Q}$ is the set of good matches with the same blue and green values. We represent 255^2 possible blue and green combinations with 51^2 bins to reduce space requirements. We use 255 bins for the red channel.

K is the kernel associated with Gaussian white noise. Note that the computation of mean-shift superpixels and non-local mean are also based on this regressor. Pixel p is deemed to be an incompatible color if $|r_p^{NW} - \hat{r}_p|$ is above a certain threshold λ. In our work, we set $\lambda = 0.3$ for intensity in the normalized range of 0 to 1. We design our colorization algorithm with a longer range than that for diffusion (101×101 instead of 21×21), and it helps to substantially reduce coloring artifacts. Two representative results are shown in the middle column in Figure 4.

8. Results

We ran our experiments on a laptop with a single core (1.6 GHz) and 2 GB of RAM. The code is that of MATLAB with certain functions implemented in C++. It takes on average between 4-10 minutes to process an image (which is first scaled to 640×480). If we only apply the rough alignment, the colorization and the incompatible color detection (referred as "MSF+col"), the process takes between 2-5 minutes. Note also that this code can be easily parallelized since most of the process are done on the left and right views independently.

To evaluate the quality of our results, we ran our experiments using stereo images and videos collected over about two years by one of the authors using FujiFilm FinePix REAL 3D W1 camera and Aiptek 3D-HD camcorder. Here we have ground truth, with the anaglyphs synthetically generated from the stereo pairs. Note that both capture devices were deliberately not calibrated for this work. We also show results of our method on images available online (including those recently taken of Mars); there is no ground truth associated with these images.

Comparison with *Deanaglyph*. This tool was released by 3dtv; it reconstructs the right image given the anaglyph and the left image. Since *Deanaglyph* assumes the left image is known, we show results only for the right image (our algorithm still computes both images) in Figure 5. Note the visible artifacts generated by *Deanaglyph*; it also crops out some amount of the border pixels.

Comparison with Bando et al. [1]. We ran our algorithm on inputs captured using the camera described in [1] (we used their image and code to generate their result). Because the blue and green channels are shifted as well, we matching the red channel to the blue and green independently. We then apply the same colorization algorithm. As shown in Figure 6, we obtained comparable results (though with less apparent edge artifacts) with the same set of parameters as used to reconstruct the other anaglyphs.

Quantitative results on our dataset. We use our datasets ("CityA" with 94 images and "CityB" with 88 images of indoor and outdoor scenes) to evaluate the effectiveness of our algorithm. Here we have ground truth, from which the input anaglyphs are generated and processed. The quality measure we compute is Peak Signal-to-Noise Ratio (PSNR): Given an image I and its reconstruction $\hat{I}$, the PSNR measure is equal to $PSNR = 20\log_{10}(max(I)) - 10\log(MSE)$, where $MSE = \|I - \hat{I}\|_2^2$.

The computed PSNR values of our algorithm are shown in Table 1. We see that our method performs better than the baseline. Note that recolorizing occluded regions does not improve the PSNR significantly, mostly because the areas occupied by occluded regions are typically small (but obvious if colorized incorrectly).

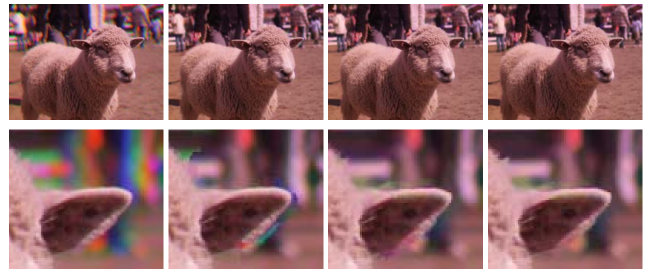

Input [1] MSF+Col Ours (final)

Figure 6. Comparison with Bando et al. [1] on images taken with their camera. "MSF+Col" refers to using our ASIFT-Flow (rough matching) and colorization. The right column is the result of applying our full algorithm. Notice that the results of our technique have less apparent edge artifacts.

Anaglyph Left Right

Figure 9. A representative failure case. The red and white part of the flag appears as uniform in the red channel in the left view, so registration in that area is less reliable.

Qualitative results and robustness. Figure 7 shows a variety of results for anaglyphs found from different online sources, including one from a comic book. These examples show that our method can work on low-quality images, and seems robust to compression artifacts. Figure 8 shows that our algorithm behaves well despite asymmetric occlusion (finger in one view but not the other), blur, or low light.

Failure cases. The most representative failure case is shown in Figure 9. Here, our algorithm fails on part of the flag because the white and red colors produces an almost constant red distribution on the left view. This causes partially incorrect transfer of blue and green to the left view. Our algorithm also does not work well with superimposed layers; other problematic cases include large disocclusions and thin structures.

9. Extension to video

Our algorithm can be easily extended to process video. To reduce flickering effects, take into account temporal information (in the form of optical flow across successive frames). Unfortunately, processing all the pixels at once is both compute- and memory-intensive.

Figure 5. Comparison with *Deanaglyph* (http://www.3dtv.at/Knowhow/DeAnaglyph_en.aspx).

Dataset	# Images	View	SIFT-Flow	ASIFT-Flow	ASIFT-Flow + Col	Ours - Occ	Ours
CityA	94	left	20.8	21.7	28.2	28.5	**28.6**
		right	21.2	22.0	29.1	29.3	**29.5**
CityB	88	left	20.5	22.3	30.2	**30.7**	**30.7**
		right	19.9	21.6	30.9	31.3	**31.4**

Table 1. Quantitative results in PSNR. (a) SIFT-Flow, (b) ASIFT-Flow (coarse matching), (c) ASIFT-Flow (coarse matching) and colorization, (d) Ours without handling incompatible colors, (e) Ours. The best number on each row is shown in bold. Examples from this dataset can be found in the supplementary file.

For efficiency reasons, we perform rough channel alignment each frame independently. We impose additional criteria on good correspondences, that of *temporal match reciprocity*: two pixels connected by the optical flow between two consecutive frames of the left view are matched to pixels of the right view that are also connected by the optical flow. Let $O^R_{t \mapsto t+1}$ be the optical flow from the frame t to $t+1$ on the right view. The additional criteria for a pixel i of the t-th frame of the left view are $O^R_{t \mapsto t+1}(M_{L \mapsto R}(i)) == M_{L \mapsto R}(O^L_{t \mapsto t+1}(i))$ as well as the right view counterpart.

Our colorization algorithm is extended to videos by computing similarity matrices within a frame W_t and between consecutive frames, $W_{t,t+1}$. The similarity matrix within a frame is similar to the one used it the case of images. Given a pixel i and its optical flow $O_{t \mapsto t+1}(i)$, the entries $W^{ij}_{t,t+1}$ of similarity matrix between consecutive frames are zero if in frame $t+1$, the two pixels $O_{t \mapsto t+1}(i)$ and j are not within 10 pixels of each other. Otherwise $W^{ij}_{t,t+1}$ is equal to:

$$\exp(-\gamma \| I_t(i) - I_{t+1}(j) \|_2^2) \delta(\| I_t(i) - I_{t+1}(j) \|_1 \leq \lambda_I).$$

We define our similarity matrix W over the whole sequence as the block matrix with W_t on the diagonal and $W_{t,t+1}$ on the second diagonal. We define the Laplacian matrix $L = I - D^{-1}W$ as before. We use a temporal window approach where each frame is colorized given its consecutive frames. This block coordinate descent scheme converges to the global minimum since the cost function is strongly convex and is linear in the number of pixels to colorize.

Figure 10 shows results for an anaglyph video, which illustrate the importance of temporal information on preventing flickering effects caused by inconsistent colors across time. If the frames are processed independently, the resulting color inconsistencies tend to be local and minor, but noticeable.

Figure 10. Results for an anaglyph video. Top row: three frames reconstructed independently. The highlighted areas (dotted ellipses) have inconsistent colors across time. Bottom row: results using temporal information. The colors are now more consistent. More examples are shown in the supplementary material.

10. Concluding remarks

We have described a new technique for reconstructing the stereo color pair from either an anaglyph image or video. Current techniques cannot be used as is because of the unique problem of matching across different color channels, transferring only specific color channels, and making sure inappropriate colors do not appear in either reconstructed view. We carefully adapted both SIFT-Flow [14] and Levin et al.'s [11] colorization technique to ensure good performance, which is evidenced in our results.

Future work includes refining object edges (perhaps using principles of matting) and adding object-level reasoning to overcome cases of ambiguity (as in the case of the red-and-white flag in Figure 9).

Acknowledgements. The work done by the first author was partially supported by the European Research Council (SIERRA and VIDEOWORLD projects).

Anaglyph Left Right Anaglyph Left Right

Figure 7. Examples of stereo pair reconstruction. We are able to handle object disocclusions and image boundaries to a certain extent. More examples can be found in the supplementary file.

Anaglyph Left Right Anaglyph Left Right

Figure 8. Robustness to asymmetric occlusion (left) and blur and low-light conditions (right). More examples can be found in the supplementary file.

References

[1] Y. Bando, B. Chen, and T. Nishita. Extracting depth and matte using a color-filtered aperture. *ACM Transactions on Graphics*, 27(5):134, 2008. 2, 6

[2] A. Y.-S. Chia, S. Zhuo, R. K. Gupta, Y.-W. Tai, S.-Y. Cho, P. Tan, and S. Lin. Semantic colorization with internet images. *ACM Transactions on Graphics*, Dec. 2011. 4

[3] H. G. Dietz. Reprocessing anaglyph images. In *SPIE EI*, 2012. 1

[4] W. Dong, G. Bao, X. Zhang, and J.-C. Paul. Fast local color transfer via dominant colors mapping. In *ACM SIGGRAPH Asia*, 2010. 2

[5] Y. HaCohen, E. Shechtman, D. B. Goldman, and D. Lischinski. Non-rigid dense correspondence with applications for image enhancement. *ACM SIGGRAPH*, 30(4):70:1–70:9, 2011. 2, 3, 4

[6] Y. Heo, K. Lee, and S. Lee. Illumination and camera invariant stereo matching. In *CVPR*, pages 1–8, 2008. 2

[7] H. Hirschmuller. Stereo processing by semiglobal matching and mutual information. *IEEE TPAMI*, 30(2):328–341, Feb. 2008. 2

[8] T. Horiuchi and S. Hirano. Colorization algorithm for grayscale image by propagating seed pixels. In *ICIP*, 2003. 4

[9] R. Irony, D. Cohen-Or, and D. Lischinski. Colorization by example. *Eurographics Symp. on Rendering*, 2005. 2

[10] J. Kim, V. Kolmogorov, and R. Zabih. Visual correspondence using energy minimization and mutual information. In *ICCV*, 2003. 2, 3, 4

[11] A. Levin, D. Lischinski, and Y. Weiss. Colorization using optimization. In *ACM SIGGRAPH*, 2004. 1, 2, 4, 5, 7

[12] Y. Li, E. Adelson, and A. Agarwala. Scribbleboost: Adding classification to edge-aware interpolation of local image and video adjustments. *Computer Graphics Forum*, 27(4), 2008. 2

[13] C. Liu. *Beyond Pixels: Exploring New Representations and Applications for Motion Analysis*. MIT, Dept. of EECS, 2009. 2

[14] C. Liu, J. Yuen, A. Torralba, J. Sivic, and W. T. Freeman. Sift flow: Dense correspondence across different scenes. In *ECCV*, 2008. 1, 2, 3, 7

[15] Q. Luan, F. Wen, D. Cohen-Or, L. Liang, Y.-Q. Xu, and H.-Y. Shum. Natural image colorization. In *Eurographics Symp. on Rendering*, June 2007. 2

[16] I. Omer and M. Werman. Color lines: image specific color representation. In *CVPR*, pages 946–953, 2004. 2

[17] F. Pitie and A. Kokaram. The linear monge-kantorovitch linear colour mapping for example-based colour transfer. In *IET CVMP*, 2007. 2

[18] E. Reinhard, M. Ashikhmin, B. Gooch, and P. Shirley. Color transfer between images. *IEEE CG&A*, 2001. 2

[19] D. Scharstein and R. Szeliski. A taxonomy and evaluation of dense two-frame stereo correspondence algorithms. *IJCV*, 47(1):742, May 2002. 2

[20] T. Welsh, M. Ashikhmin, and K. Mueller. Transferring color to greyscale images. In *ACM SIGGRAPH*, 2002. 2

[21] X. Xiao and L. Ma. Color transfer in correlated color space. In *VRCIA*, 2006. 2

[22] L. Yatziv, G. Sapiro, R. Lukac, and K. N. Plataniotis. Image and video colorization. In *Color Image Processing: Methods and Applications*. CRC/Taylor and Francis, 2006. 2, 4